

## Spectral properties, magnetic fields, and dust transport at lunar swirls

Ian Garrick-Bethell<sup>\*</sup>, James W. Head III, Carle M. Pieters

Brown University, Department of Geological Sciences, 324 Brook Street, Providence, RI 02912, United States

### ARTICLE INFO

#### Article history:

Received 21 January 2010

Revised 23 November 2010

Accepted 23 November 2010

Available online 23 December 2010

#### Keywords:

Reiner Gamma

Swirls

Magnetism

Dust

### ABSTRACT

Lunar swirls are albedo anomalies associated with strong crustal magnetic fields. Swirls exhibit distinctive spectral properties at both highland and mare locations that are plausibly explained by fine-grained dust sorting. The sorting may result from two processes that are fairly well established on the Moon, but have not been previously considered together. The first process is the vertical electrostatic lofting of charged fine dust. The second process is the development of electrostatic potentials at magnetic anomalies as solar wind protons penetrate more deeply into the magnetic field than electrons. The electrostatic potential can attract or repel charged fine-grained dust that has been lofted. Since the finest fraction of the lunar soil is bright and contributes significantly to the spectral properties of the lunar regolith, the horizontal accumulation or removal of fine dust can change a surface's spectral properties. This mechanism can explain some of the spectral properties of swirls, accommodates their association with magnetic fields, and permits aspects of weathering by micrometeoroids and the solar wind.

© 2010 Elsevier Inc. All rights reserved.

## 1. Swirl models and observations

### 1.1. Previous swirl models

Bright swirl-shaped features on the Moon have remained one of the most enigmatic lunar geologic features (El-Baz, 1972; Hood and Schubert, 1980; Schultz, 1976; Schultz and Srnka, 1980). Generally, lunar swirls have high albedo, low optical maturity, and often exhibit dark lanes that interweave with brighter features (Fig. 1). Swirls have morphology that varies between diffuse patches and sinuous curves (Blewett et al., 2007). Swirls are also correlated with magnetic anomalies (Hood and Williams, 1989; Richmond et al., 2005), some of which are antipodal to major basins. If there is any topographic relief at swirls, it must be below tens of meters, since it is not detectable with existing photographic data sets.

No completely satisfactory model for swirl formation has emerged (Lucey et al., 2006). One class of hypotheses suggests recent (<100 Myr) impacts (Pinet et al., 2000; Schultz and Srnka, 1980; Starukhina and Shkuratov, 2004; Shkuratov et al., 2010) scoured away dark, mature material to reveal fresh unweathered soil, but these models do not easily explain the swirl association with magnetic anomalies (Richmond et al., 2005; Nicholas et al., 2007). Alternatively, Hood and Schubert (1980) proposed that local magnetic fields may form mini-magnetospheres that stand off the solar wind, thereby preventing maturation of the underlying soil.

Although the impact model has some deficiencies, a possible correlation between swirls and fresh craters has been noted, such as at Goddard A (Schultz and Srnka, 1980), and the albedo anomaly near Descartes (Blewett et al., 2005a,b) (Section 2.3). A possible explanation may be that the solar wind stand-off hypothesis is correct, and fresh material emplaced in magnetized regions weathers more slowly than surrounding non-magnetized regions, thereby forming a swirl. Nonetheless, after billions of years, newly emplaced material in magnetic regions may eventually reach a state of background maturity. Thus regions with fairly strong magnetic anomalies may have no swirls if they have not received any relatively fresh material. An alternative explanation to the possible correlation with fresh craters, however, is that fresh craters near swirls only appear to be relatively fresh because the swirl forming process affects spectral maturity parameters, and these craters are in fact older than they appear to be.

If correct, the solar wind stand-off model would elegantly explain both the brightness of swirls and their association with crustal magnetism, and it has therefore emerged as a leading candidate for swirl formation. However, there are a number of difficulties with the model that have not yet been fully addressed. For example, one objection is that micrometeoroids are unimpeded by magnetic fields (Richmond et al., 2003) and cause the same space weathering effects in timescales of ~100 Myr for the present micrometeoroid flux (Sasaki et al., 2001, 2003; Brunetto et al., 2006), still less than the 2–4 billion year old background surface ages of most swirls. While this is a valid concern, it is possible that the solar wind weathering time may be rapid (~1 Myr) (Hapke, 2001; Brunetto and Strazzulla, 2005; Strazzulla et al., 2005; Vernazza et al., 2009), and mere modifications in the rate of solar

<sup>\*</sup> Corresponding author. Present address: University of California, 1156 High Street, Santa Cruz, CA 95064, United States.

E-mail address: [igarrick@ucsc.edu](mailto:igarrick@ucsc.edu) (I. Garrick-Bethell).

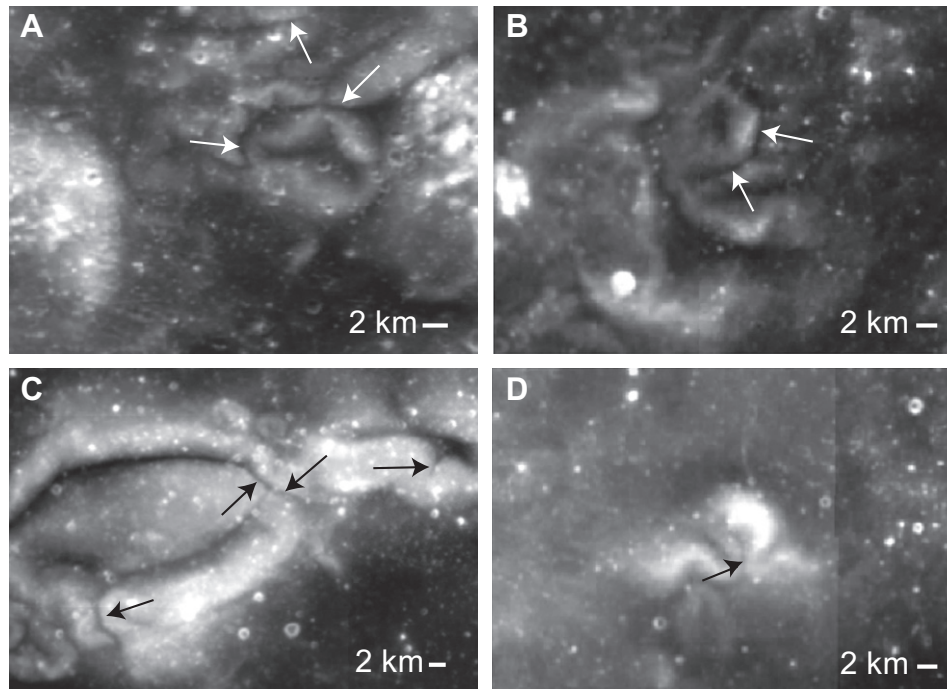


**Fig. 1.** Dark lanes in lunar swirls (750 nm Clementine reflectance), indicated by arrows. (A) Mare Ingenii ( $-35.0^{\circ}\text{S}$ ,  $163.2^{\circ}\text{E}$ ), (B) Mare Marginis ( $13.3^{\circ}\text{N}$ ,  $84.4^{\circ}\text{E}$ ), (C) Reiner Gamma swirl ( $7.5^{\circ}\text{N}$ ,  $301.5^{\circ}\text{E}$ ), (D) region south of Reiner Gamma swirl ( $-1.0^{\circ}\text{S}$ ,  $298.7^{\circ}\text{E}$ ).

wind weathering may be sufficient to cause surface brightening (Hood and Williams, 1989). Another concern with the stand-off model is that many swirls, such as those at Mare Marginis (Richmond and Hood, 2008), have weak magnetic anomalies compared to the center of Reiner Gamma swirl, yet Reiner Gamma is the only swirl for which deflection of protons has been modeled (Hood and Williams, 1989). In addition, a reduced solar wind flux also does not easily explain possibly anomalous photometric properties of Reiner Gamma (Kreslavsky and Shkuratov, 2003; Pinet et al., 2004; Chevrel et al., 2006; Kaydash et al., 2009), which suggest a unique regolith microstructure. Radar observations also indicate anomalous surface roughness at the 3.8 cm scale, but not at the 70 cm scale, at the putative Descartes swirl (Zisk et al., 1972; Thompson et al., 1974; Blewett et al., 2005a,b). Reiner Gamma may also exhibit anomalous 13-cm-scale roughness (Campbell et al., 2006).

The outline of the paper is as follows. In Section 2 we present an analysis of near-surface magnetic field strengths at swirls, as well as new spectral observations of lunar swirls. In Section 3 we present a model for swirl formation by dust transport. In Section 4 we discuss the implications of the dust transport model, as well as an alternative interpretation of the spectral data. In Section 5 we conclude the paper.

## 2. Magnetic and spectral properties of swirls

### 2.1. Magnetic field strength at swirls

Knowledge of the near-surface magnetic field strength at lunar swirls would be useful in determining both the swirl forming process and the origin of the magnetic anomaly. For example, the near-surface field strength can help constrain the volume magnetization and distribution of magnetized material, which in turn relates to how the anomaly formed. Previously, only inversions from orbital spacecraft data collected above  $\sim 20$  km have been used to constrain the near-surface field strength (Hood et al., 1979; Hood,

1980; Kurata et al., 2005). Below we explain how unique morphologic features of swirls can be related to the near-surface field strength, and with a better model of the plasma interaction with lunar magnetic fields, provide a means of measuring surface field strengths.

Inside the high albedo areas of many swirls are dark lanes where the swirl forming process apparently does not operate. The thickness of these lanes may be related to the magnetic field strength. For example, if the solar wind stand-off hypothesis is correct, dark lanes suggest the solar wind is being focused into an otherwise wind-deflected region (Fig. 1) (Hood and Schubert, 1980). The focusing width is limited by the proton gyro-diameter, which in turn can be related to the near-surface field strength. Hood and Williams (1989) performed simple, Lorentz force-only simulations of protons incident on arrangements of buried magnetic dipoles, and found focusing regions of  $\sim 2$  km thickness for surface fields of 2800 nT. Swirls, however, often exhibit dark lanes with thicknesses on the order of 600 m, Fig. 1, which would imply surface fields of the order of 9000 nT, if only the Lorentz force was important.

For at least two reasons, however, more detailed models of the solar wind interaction with magnetic fields are required before lanes can be used to measure field strength, if the solar wind hypothesis is correct. Firstly, charge separation electric fields and proton–electron momentum transfer will reduce the proton gyro-diameter to a value intermediate between the electron and proton values (Hood and Schubert, 1980; Hood and Williams, 1989). Secondly, it is possible the precipitation of particles along open magnetic field lines that connect to the interplanetary magnetic field will result in the surface impact of particles with low pitch angles and gyro diameters. A similar process produces aurorae on the Earth (Zhang et al., 2007), Mars (Bertaux et al., 2005; Lundin et al., 2006), and Jupiter (Bhardwaj and Gladston, 2000). Some of the martian aurorae occur at clefts and boundaries between magnetic anomalies, and some even exhibit a sinuous appearance.

Previous inversions for the near-surface field strength at Reiner Gamma found fields of  $\geq 1000$  nT (Hood et al., 1979) and  $\sim 1000$  nT

in (Kurata et al., 2005) (using their 11 km depth buried dipole). This value would be in agreement with the Lorentz force estimate from dark lanes and proton gyrodiameters, if the combination of the two plasma effects described above resulted in about an order of magnitude gyrodiameter reduction.

If 1000 nT fields exist at the surface, what volume magnetization is required? If the Reiner Gamma anomaly is modeled as a horizontal disk of diameter 10 km, with a thickness of 1 or 10 km, an axial field of 1000 nT is produced by magnetizations of 10 or 1 A/m, respectively, using equations from Collinson (1983). Larger diameter disks require higher magnetizations. These magnetizations are in reasonable agreement with minimum magnetizations of 1 and 0.1 A/m for layer thicknesses of 1 and 10 km, respectively, derived from an ideal bodies approach (Nicholas et al., 2007). Magnetizations of 0.1–1 A/m would be among the most magnetic samples measured. For example, Apollo breccias 62235 and 15498 have magnetizations of 0.3 and 0.2 A/m, respectively, and are the two most magnetic samples reported by the review in (Fuller and Cisowski, 1987), aside from possibly contaminated samples.

In Section 3 we will develop a new theory for swirl formation, motivated in part by the spectral data below. This new theory, if correct, may give further insight into magnetic field strengths at swirls, and therefore the nature of lunar magnetic anomalies in general.

## 2.2. Spectral properties of lunar swirls

Several characteristic spectral properties of swirls can be discerned from detailed analysis of Clementine five band UV–VIS data. The first is that swirls show an apparent space weathering trend different from the normal background trend of local maturity. With Clementine data, lunar space weathering trends can be evaluated by plotting 950/750 nm reflectance (low values of which are a proxy for strong ferrous band strength at ~1000 nm) vs. 750 nm reflectance (albedo) (Lucey et al., 2000). A large compositionally homogeneous area of the lunar surface will nominally display a linear trend in this plot. For mare regions, higher maturity pixels are found in upper left, and immature pixels are found in the lower right, herein called the “maturity trend.” This trend is illustrated as Trend 2 in Fig. 3a, for the region in Fig. 2a enclosed by the blue labeled rectangle. Trend 2 is as expected for well-developed soils (low albedo, upper left) and small, fresh craters in the area (high albedo, lower right). However, for both highland and mare swirls, brighter, immature portions of swirls do not simply follow such a maturity trend, but form new linear trends that are displaced to higher 750 nm values and slightly lower 950/750 ratios (Fig. 3). This trend is illustrated as Trend 1 in Fig. 3a.

In some ways, Trend 1 is similar to what is observed after a small highlands component of soil is added to a mare soil. For example, Staid and Pieters (2000) found that when mare locations were contaminated with highlands ejecta, their maturity trend was broadened and displaced in the same direction in 750 nm reflectance as described above. Bell and Hawke (Bell and Hawke, 1987) found that Reiner Gamma was best modeled as a mixture of immature mare material and a small component of highlands material. Although there is some evidence that Reiner Gamma may have received ejecta from craters in the highlands (Hood et al., 1979), there is no reason to believe that this same apparent highlands component could be explained by similar processes at all of the other mare swirls (Figs. 2 and 3), or that the ejecta’s influence should be so systematic across regions within Reiner Gamma.

Our interpretation of this apparent highlands component is that it may be an enrichment in fine-grained material, which may also be slightly enriched in feldspar. Unusually abundant fine-grained material could create such a feldspathic enrichment because the finest fraction of both mare and highland soils are naturally slightly feldspar rich (Taylor et al., 2001; Pieters and Taylor, 2003).

Another characteristic spectral property of swirls is that transects through prominent mare swirls often show a strong increase in continuum slope or “redness” (herein defined as 750/415 nm) around the periphery of the swirl, previously referred to as a “red halo” at Reiner Gamma (Bell and Hawke, 1987; Pinet et al., 2000). This abnormally high redness compared to background values is most obvious at Reiner Gamma, the swirl north of Reiner Gamma, and swirls at Mare Ingenii (red arrows in Fig. 4e, c, and a, respectively). In contrast, the central bright parts of swirls exhibit a decrease in redness (Fig. 4a–f), and here redness is anti-correlated with albedo and correlated with high band strength. Note that the central part of Reiner Gamma (Fig. 4e, black arrow) has only moderate redness and band strength at its center, suggesting the swirl forming process may be less effective there. Central regions of highland swirls show only a decrease in redness relative to background values (Fig. 4d), and do not appear to have a red halo as do most mare swirls.

The interior “dark lanes” and the periphery of some strong swirls, such as the central part of Reiner Gamma, do not show an appreciable increase in band strength or albedo, at least relative to the local background. For example, the light blue and black *L*-labeled rectangles in Figs. 2e and 3e represent dark lanes with pixels that fall within the background mare trend (blue labeled rectangle in Fig. 2e). Several exceptions to this can be found in smaller swirls south of the main Reiner Gamma feature, where magnetic fields are weaker. One example is shown in Figs. 2e and 3e, as the red colored trend labeled *L*, which is slightly darker than the background soil, but not darker than some other soils south of Reiner Gamma. Generally, however, the dark lanes appear similar to background material in the region.

## 2.3. Application to Descartes albedo anomaly

The above spectral characteristics of lunar swirls are useful for distinguishing swirls from other albedo anomalies. For example, we can examine in some detail the Descartes region albedo anomaly (Fig. 2f). The Descartes albedo anomaly is a bright, immature feature between two fresh craters (Dolland D and Descartes E) in lunar highlands terrain, with nearly overlapping ejecta deposits, and its status as a swirl is uncertain (Blewett et al., 2005a,b). The region exhibits anomalous 3.5 cm radar reflectance (Zisk et al., 1972).

A transect through the center of the bright patch reveals broad changes in albedo, band strength, and redness (Fig. 4f, transect 2) that are similar to Airy swirl, also located in the highlands (Fig. 4d). A transect an equal distance away from Dolland D, but in the opposite direction of the bright patch, reveals a much smaller change in spectral characteristics (transect 1). A transect an equal distance from Descartes E, but again in the opposite direction of the bright patch, reveals almost no change in spectral properties compared to the background (transect 3). A transect through Dolland D, the center of the bright region, and Descartes E reveals a region of nearly constant but anomalous band strength, redness, and albedo, bounded by a slope break indicated with \* in Figs. 4f and 2f. If the bright patch were due entirely to overlapping ejecta deposits, one might expect a decay of the spectral anomalies near the two craters’ midpoint, but this is not observed. The reason that the two craters appear fresh may partially be a result of an underlying magnetic anomaly and swirl forming mechanism, and not just a coincidence of two nearby fresh craters. Further measurements of spectral and other physical properties of the Descartes region may resolve the issue (Section 4).

## 3. Dust transport model for swirl formation

To explain the immaturity and brightness patterns of swirls, without requiring stand-off of the solar wind, we propose an

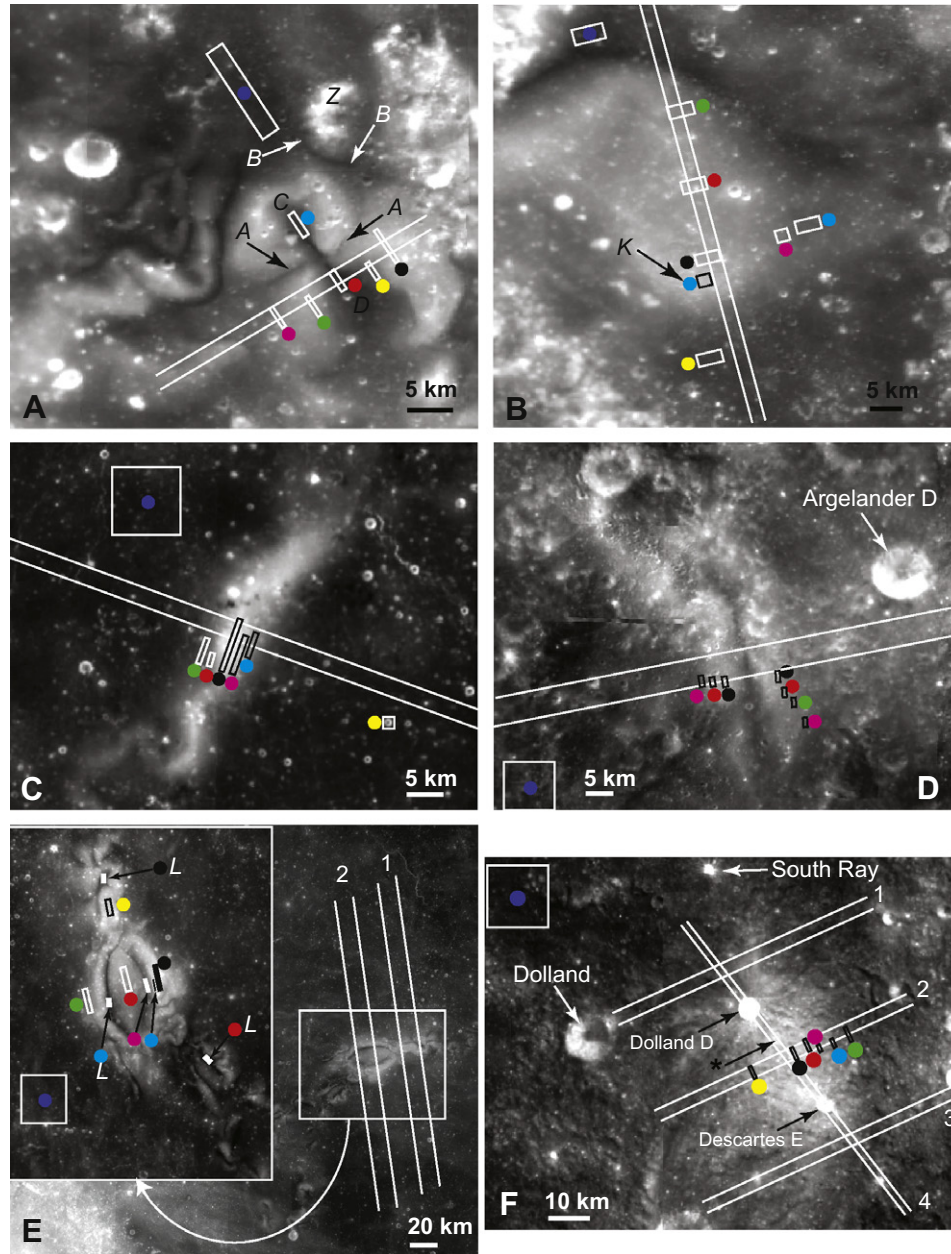


**Fig. 2.** Mare and highland lunar swirls (750 nm Clementine reflectance). White and black rectangles and their associated colored circles indicate regions where approximate band strength and albedo are plotted in Fig. 3. Rectangles with labels K and L in parts B and E, respectively, indicate regions with repeated colors. Areas between white lines have been averaged to generate the transects in Fig. 4. North is up. (A) Mare Ingenii ( $-33.6^{\circ}\text{S}$ ,  $163.1^{\circ}\text{E}$ ), (B) Mare Ingenii, south of part A ( $-36.1^{\circ}\text{S}$ ,  $165.4^{\circ}\text{E}$ ), (C) north of Reiner Gamma swirl ( $-10.7^{\circ}\text{S}$ ,  $304.9^{\circ}\text{E}$ ), (D) west of Airy crater ( $-18.1^{\circ}\text{S}$ ,  $3.4^{\circ}\text{E}$ ), (E) Reiner Gamma swirl ( $7.5^{\circ}\text{N}$ ,  $301.5^{\circ}\text{E}$ ), (F) Descartes swirl ( $-17.1^{\circ}\text{S}$ ,  $9.9^{\circ}\text{E}$ ), location marked with \* is shown in Fig. 4f.

alternative model that involves electric fields at swirls. Electric fields have been used to explain dust transport on asteroids (Berg, 1978; Hughes et al., 2008; Riner et al., 2008) and the Moon (Berg et al., 1976; Page and Carruthers, 1978; Rennilson and Criswell, 1974; Severnyi et al., 1975; Stubbs et al., 2006; Zook and McCoy, 1991; Zook et al., 1995). Electric fields are often produced by plasma interactions with magnetic fields (Alfvén and Fälthammer, 1963), such as in the Earth's aurora (Ergun et al., 2004; Hull et al., 2003; Raadu, 1989). Neugebauer (Neugebauer et al., 1972) was the first to infer that electric fields are produced by lunar crustal magnetic anomalies, and the process is also discussed in Hood and Schubert (1980) and Hood and Williams (1989).

### 3.1. Charge separation at magnetic anomalies

When solar wind protons and electrons encounter a weak crustal magnetic field, some electrons are reflected before reaching the surface due to the magnetic mirroring effect, assuming the frequency of the magnetic field change is less than the electron gyrofrequency (adiabatic assumption) (Lin, 1979; Lin et al., 1998). For example, surface fields of 1–5 nT reflect of  $\sim 25$ –50% incident electrons (Halekas et al., 2001) (most swirls have fields of  $>1$  nT at 20–30 km altitude (Hood et al., 2001; Blewett et al., 2005a,b)). However, the more massive and slower solar wind protons have a lower gyrofrequency, and their less adiabatic motion will cause them to more deeply penetrate the magnetic field. The differential

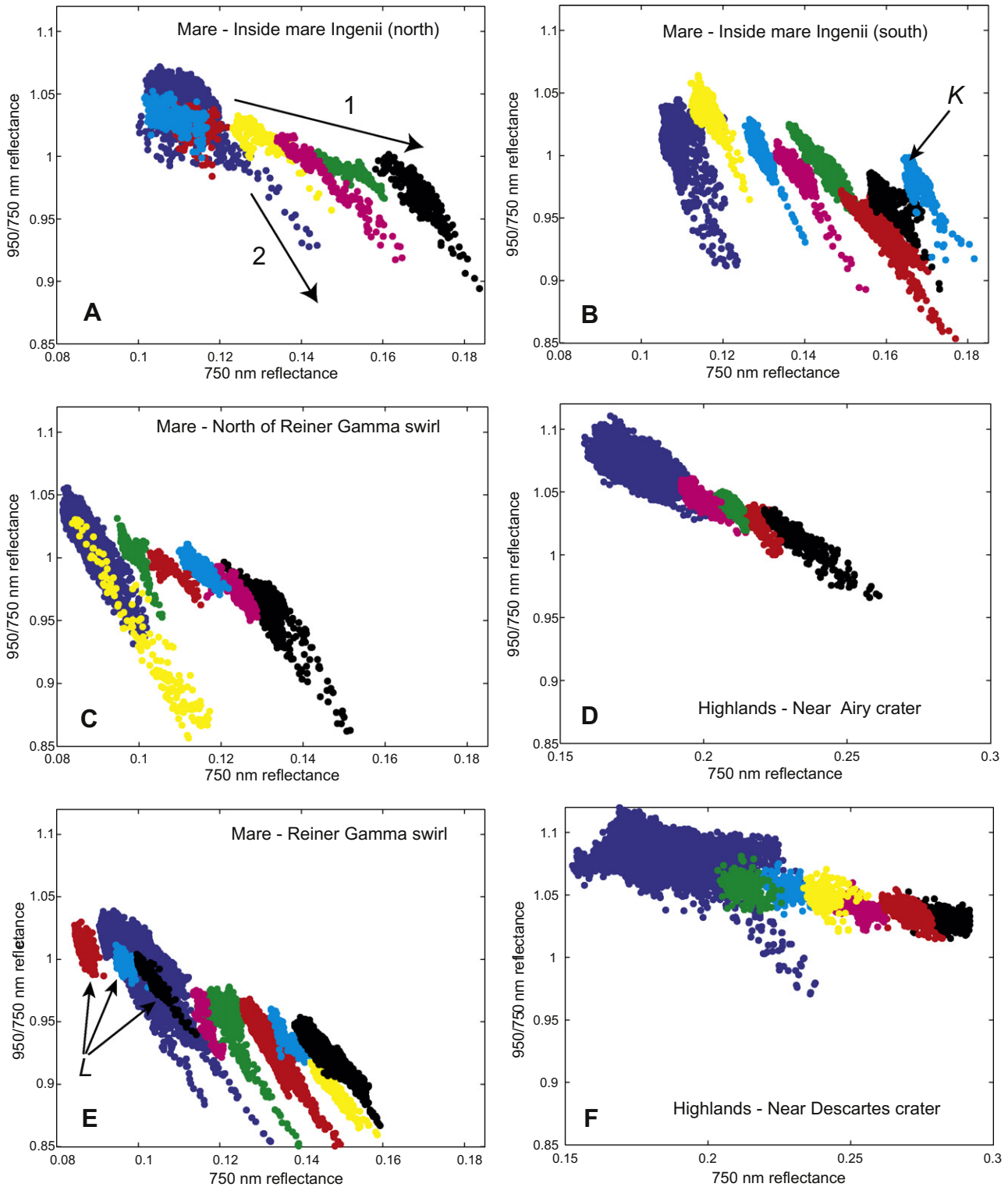


**Fig. 3.** Approximate band strength (950/750 nm) vs. albedo (750 nm) for the regions in swirls presented in Fig. 2. The data are taken from the white and black rectangles in Fig. 2, with the color of the data points corresponding to the colored circle labels at each rectangle. Labels *K* and *L* in parts B and E, respectively, indicate regions with repeated colors. The two trends of swirl maturation and normal maturation, are illustrated 1 and 2 in part A, respectively. Yellow portion of part C is not located at a swirl, but is shown to illustrate the normal background maturity trend for a fresh crater. In part D the two sets of magenta, red, and black rectangles have been averaged together.

penetration of protons and electrons causes a positive charge excess above the surface (Neugebauer et al., 1972; Siscoe and Goldstein, 1973; Goldstein, 1974; Burke and Reiff, 1975; Clay et al., 1975; Reiff, 1975; Reiff and Burke, 1976). Calculations suggest the charge excess is not likely to be shorted out by conduction through the lunar photoelectron layer or lunar surface (Siscoe and

Goldstein, 1973). Note that if the magnetic field is strong enough to form a magnetopause, charge separation may still occur (Ferraro, 1952; Willis, 1971; Hood and Schubert, 1980; Hood and Williams, 1989).

The electric potential created by charge separation is known as a plasma double layer, a well-known state where quasi-neutrality

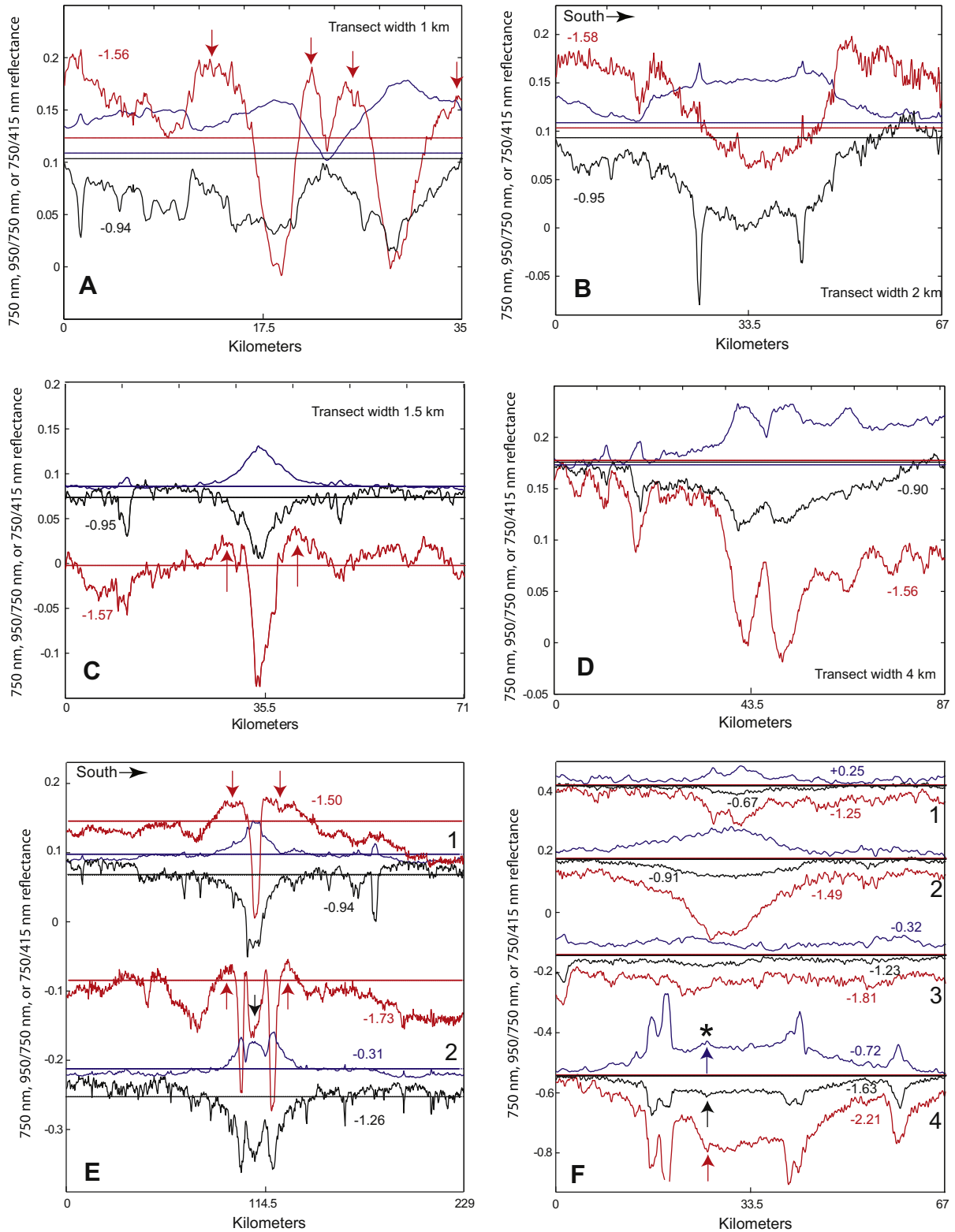


**Fig. 4.** Transects across lunar swirls in band strength (black), albedo (blue), and redness (750/415 nm, red), for the swirls presented in Fig. 2. Transects represent averages of values between the white lines in Fig. 2, and the width of this region is indicated in each figure. The band strength and redness transects have been vertically shifted to facilitate comparisons. The values on the vertical axis apply to the albedo transects. Values for the other two transects are offset from the albedo by the numbers near each transect. In parts E and F, some of the albedo transects have also been offset, such that all transects are relative to the albedo of the unlabeled albedo transect. Solid horizontal lines represent the mean values for the rectangular background regions in Fig. 2 (labeled with blue circles), using the same offsets as the transects. The background region for part B is the same as the one used for part A, since they are both located in Mare Ingenii, and the limits of the swirl in part B are uncertain. Arrows in parts A, C and E are used for discussion in Section 2.2. Location labeled with \* in part F is shown in Fig. 2f. Abscissa scale for transect 4 in part F is 0 to 88.1 km.

does not exist. Plasma double layers have been studied in the context of laboratory, magnetospheric, and space plasmas (Schamel, 1986; Raadu, 1989; Charles, 2007). The typical thickness of double layers is limited to <100 Debye lengths (Charles, 2007), or <1 km in the solar wind. The generation of charge separation and a positive electric potential in a plasma with increasing magnetic field strength has recently been demonstrated in a laboratory experiment (Takahashi et al., 2008), analogous to the lunar phenomenon. In this experiment, the authors also observed reflection of protons entering the high magnetic field region, due to the positive electric field of the double layer. These experiments may have applications to observations of proton reflections on the Moon (Saito et al., 2009).

The equilibrium near-surface charge excess due to the magnetic field will be a balance between the penetration of protons, and the downwards draw of electrons due to the positive charge, in spite of the magnetic mirror (a requirement for zero net current) (Reiff, 1975). The equilibrium charge separation voltage depends critically on the field geometry and strength, and the ambient plasma conditions (Reiff, 1975). An upper limit is of the order of the proton energy, since higher voltages would reflect nearly all protons. Assuming 1 keV solar wind proton energies, and separation of charge over horizontal scales of  $\sim 10$  km (e.g. the swirl scale of Mare Ingenii, Fig. 2a), local electric fields would be <100 mV/m. Smaller length scales would produce higher electric fields.

Charge separation has been inferred from solar wind observations at the Apollo 12 and 14 landing sites. At the 38 nT surface field at the Apollo 12 site (Dyal and Sonett, 1970; Clay et al., 1975) nonthermal electrons were accelerated towards the solar wind spectrometer, suggesting that they were accelerated by a local positive electric anomaly of the order 50–120 eV (Goldstein, 1974; Clay et al., 1975). Such electron energy anomalies were not detected at the Apollo 15 site, where the local field was <6 nT (Goldstein, 1974). In addition, solar wind protons were decelerated at the Apollo 12 site by 70–150 eV, a range comparable to the electrons and interpreted to be due to a local positive electric field (Neugebauer et al., 1972; Goldstein, 1974; Clay et al., 1975). Assuming the positive potential exists over length scales similar to the magnetic anomaly,  $\sim 5$  km (Barnes et al., 1972; Neugebauer et al., 1972; Clay et al., 1975), an estimate of the maximum electric field is  $\sim 20$  mV/m, in agreement with the estimate in (McCoy, 1976). At the  $\sim 75$  nT magnetic anomaly at the Apollo 14 site (Reiff and Burke, 1976), downwelling electron fluxes of 50–70 eV were interpreted to be due to charge separation (Burke and Reiff, 1975; Reiff, 1975; Reiff and Burke, 1976). Assuming a length scale of  $\sim 1$  km at this site (Reiff and Burke, 1976), the maximum electric field would be  $\sim 50$  mV/m. Eventually, detailed modeling, laboratory experiments, and measurements of magnetic anomalies will be required to constrain the equilibrium charge separation. We note however that the Apollo 12 and 14 surface magnetic fields are relatively weak compared to swirls, and the electric fields may therefore be higher in swirl regions (although perhaps at a high altitude, next section).

### 3.2. Lofting of lunar dust

In a separate process unrelated to magnetic anomalies, fine lunar dust in sunlit portions of the Moon becomes positively charged, primarily through photoelectron emission. Under certain circumstances, such as in the deeply shadowed terminator region (Criswell, 1972), the charge buildup may be strong enough to loft grains above the surface. The existence of dust lofting is suggested by Surveyor 5–7 (Rennilson and Criswell, 1974), Lunokhod 2 (Severnyi et al., 1975) and Clementine (Zook et al., 1995) observations, Apollo 16 sky brightness measurements (Page and Carruthers, 1978), Apollo 15 and 17 solar corona measurements (McCoy,

1976), astronaut observations (Zook and McCoy, 1991), and theory (Criswell, 1972; Criswell and de, 1977; Pelizzari and Criswell, 1978; Nitter et al., 1998). Perhaps the best evidence is the surface measurement of increased fluxes of slow moving charged particles during terminator crossings at the Apollo 17 site, with the Lunar Ejecta and Meteorites Experiment package (Berg et al., 1976). A number of laboratory simulations have been performed that support various aspects of dust lofting (Sickafoose et al., 2002; Robertson et al., 2003; Colwell et al., 2009; Wang and Robertson, 2009), but none have completely simulated all aspects of the problem.

The lack of significant dust on Surveyor 3 footpad markings and on the surface of the now functioning laser retroreflectors is not necessarily evidence against dust transport or lofting (Colwell et al., 2007, 2009). Dust transport may be relatively inefficient over 2–40 years, but over geologic timescales it may become important enough for our model. Additionally, in the absence of magnetic or electric fields, a steady-state equilibrium may exist such that over short terms, no net accumulation takes place. Also, some interpretations of lunar laser ranging data do in fact suggest performance degradation due to dust accumulation (Murphy et al., 2010). Note that dust transport processes are also believed to create ponding of spectrally distinct deposits on asteroids (Hughes et al., 2008; Riner et al., 2008; Robinson et al., 2001), and horizontal electrostatic dust transport has recently been simulated in the laboratory (Wang and Robertson, 2009).

While lofted dust can explain a number of spacecraft observations, and electrostatic forces are likely at work, the details of the process or processes are not well known (Colwell et al., 2007, 2009). For example, Criswell (1972) suggests dust is stably levitated, but Colwell et al. (2009) and Stubbs et al. (2006) suggest a form of ballistic transport is also possible. Perhaps the most significant unresolved issue is how dust lifts off from the surface. Most studies imply lift-off occurs mainly in the terminator region. However, observations (Severnyi et al., 1975; Page and Carruthers, 1978) and theory (Singer and Walker, 1962a,b; Walker, 1973; Stubbs et al., 2006) also suggest it may operate globally to some extent. The estimated diameter of the lofted grains is also unclear, varying between submicron (Zook and McCoy, 1991; Colwell et al., 2009),  $\sim 10$   $\mu\text{m}$  (Rennilson and Criswell, 1974), and  $>10$   $\mu\text{m}$  (Severnyi et al., 1973). Stubbs et al. (2006) estimated that dust with a radius of 0.1–1  $\mu\text{m}$  could be lofted between tens of meters to several kilometers.

Herein we assume that dust is lofted twice a lunar day at each terminator crossing. To allow for the unknown details of the lofting processes in our model for dust transport, we explore different grain sizes and lofting times. Note that if the lofting process only operates in the terminator region, charge separation is still likely to develop if a crustal magnetic anomaly exists (Russell and Lichtenstein, 1975), and thereby produce an electrostatic potential. Furthermore, lunar dust movement has been observed  $\sim 60$  h ( $3^\circ$  at the equator) after sunrise and before sunset (Berg et al., 1976), such that dust lofted at the terminator may arrive at a more fully sunlit magnetic anomaly, where the solar wind is active and able to generate an electric field.

The altitude and detailed geometry of the charge separation region at lunar swirls is not known. For the largest swirls, if they develop full magnetospheres, the altitude may be on the order of 10 km above the surface. However, the altitude of dust lofting is also similarly unknown, ranging from centimeters (Rennilson and Criswell, 1974) to kilometers (Zook and McCoy, 1991; Stubbs et al., 2006). Therefore, it is plausible that the charge separation region interacts with charged lofted dust even at the strongest magnetic anomalies.

A final concern is the sign of the charge of lofted dust. Grains in sunlight and surrounded by minimal electron charging currents, such as at high solar illumination angles under mean solar wind

conditions, will charge positive, due to the dominance of photoelectron emission (Walker, 1973). Negative electric charging can take place in shadow in the terminator region due to the lack of photoelectron emission (Borisov and Mall, 2006; Wang and Robertson, 2009). However, the generation of substantial negative electric fields can also take place in sunlight near the terminator (Berg, 1978; Halekas et al., 2005; Farrell et al., 2007; Wang et al., 2008), such as during low sun angles or plasma conditions with high electron fluxes, leading to either stable levitation or ballistic ejection of negatively charged particles. Ultimately, it is likely that populations of both charge states exist. However, it is also at least plausible that the populations are asymmetric, because of the diversity of processes that produce each one, such that any net accumulation of dust will not be perfectly canceled by movement of oppositely charged dust. Note that charged dust may also accumulate by repulsion from a region, not just attraction.

### 3.3. Horizontal lunar dust transport

Lofted charged dust that is within or around a positive electrostatic anomaly produced by a crustal magnetic field will be either horizontally repelled or attracted towards to the anomaly. Although the distance traveled may be small during lofting and repulsion (<1–100 cm), repeated loftings may eventually transport a particle over kilometers, Fig. 5. Because the lowest mass material is preferentially lofted, the finest fraction of lunar soil will be preferentially transported. The finest fraction of lunar soil (<45 μm) is known to dominate its spectral properties (Pieters et al., 1993). Because fine-grained material is continually being created and matured in a steady-state equilibrium (McKay et al., 1974), the transport of newly created fine dust into or out of an electric anomaly would also alter the local steady-state equilibrium, and ultimately change the spectral properties of the region.

Firstly, to determine if lofting and repulsion can transport dust on the length scale of swirls, approximately 2–10 km, we calculate the total transportation distance for a dust grain assuming a variety of parameters. The total distance a grain travels,  $d$ , can be written:

$$d = N \frac{1}{2} \left( \frac{Eq}{m} \right) t^2$$

where  $N$  is the total number of lofting events and subsequent horizontal movements,  $E$  is the local electric field,  $q$  is the charge on

the dust grain,  $m$  is the dust grain mass, and  $t$  is the time the particle spends horizontally accelerating in each lofting. The equation is for 1-dimensional acceleration of magnitude  $(Eq/m)$ , multiplied by  $N$ .  $N$  can be equivalently expressed as the number of years over which the transportation takes place,  $N = P \times 2 \times 365 t_y / (29.5)$ , where  $t_y$  is the total exposure time at the surface in years, and  $P$  is the probability of lofting during both sunset and sunrise (Berg et al., 1976). We assume  $m = (4/3)\pi\rho r^3$ , where  $r$  is the dust grain radius, and  $\rho$  is the effective density, assumed to be 2000 kg/m<sup>3</sup>. We explore  $r = 1 \mu\text{m}$  and  $r = 5 \mu\text{m}$ , based on the two lofting models put forward by Stubbs et al. (2006) and (Criswell (1972), respectively. Lofted grains with  $r \ll 1 \mu\text{m}$ , as modeled in Colwell et al. (2009), are easily transported.

To estimate the efficiency of the dust transport process, we will assume that grains are charged positively, as in the case of lofting into sunlight. We do so because the voltages calculated for positive charging are usually smaller than those due to negative charging, and will therefore serve as a lower limit. Following Goertz (1989), Stubbs et al. (2006), Wang et al. (2008), we assume  $q = C\phi$ , where  $q$  is the charge on the grain,  $C$  is the capacitance and  $\phi$  is the grain voltage, with  $C \approx 4\pi\epsilon_0 r$ , where  $\epsilon_0$  is the electric constant. The grain potential will change after the grain is ejected from the sunlit surface and transitions into or out of the photoelectron layer (Nitter et al., 1998). However, the equilibrium charge in flight will be close to the lunar surface potential (Walker, 1973). Note that a similar assumption has also been made for negatively charged particles in the past (Farrell et al., 2007; Wang et al., 2008) (a detailed exploration of the time dependent charge is warranted when more information about the lofting process becomes available). Also note that this is entirely different from making the (incorrect) assumption that an individual grain's potential while at rest on the surface is the same as the total surface potential (see discussion in Singer and Walker, 1962a,b).

A range of sunlit lunar surface potentials have been previously calculated (see Halekas et al., 2008), such as +4 V (Willis et al., 1972; Stubbs et al., 2006), +9 V (Manka, 1973), +20 V (Singer and Walker, 1962a,b), <+20 V (Halekas et al., 2008), +200 V in some conditions (Reasoner and Burke, 1972), and higher values in the terminator region (Criswell and de, 1977). We assume the surface is at approximately 10 V, and therefore, assuming that the surface potential is a reasonable approximation for the potential of grains in flight, we assume  $\phi = 10 \text{ V}$ , as in Singer and Walker (1962a,b) and Walker (1973). Collective effects of multiple lofted grains

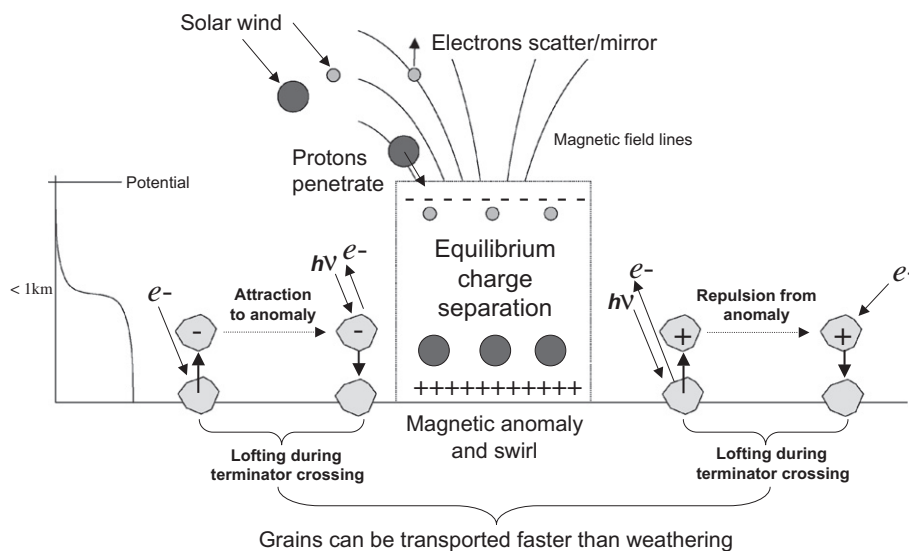


**Fig. 5.** Charge separation at magnetic anomalies produces an increasing electric potential known as a double layer. The potential increase due solely to the charge separation is sketched at the left, and ignores the photoelectron sheath or other sources of electric potential. Fine dust that is electrostatically lofted each day can be repelled or attracted to the positive potential above the surface.

may reduce the equilibrium charge from the theoretical free-space value for an individual grain, but this effect is likely small at the column densities of  $\sim 5$  grains/cm<sup>2</sup> inferred by Criswell (1972).

A lower limit on the timescale (or  $N$ ) for efficient swirl production may be calculated assuming that (i) the albedo markings are related to a lack of soil maturity (Section 3.4), and (ii) a grain must be transported the length scale of the swirl before it becomes greatly weathered. We therefore seek a lower bound on the space weathering timescale. Based on ion implantation experiments, solar wind maturation is estimated to take place within  $10^5$ – $10^6$  years of surface exposure on the Moon (Hapke, 2001; Brunetto and Strazzulla, 2005; Strazzulla et al., 2005). For a lower bound we therefore assume  $t_y = 10^5$  years. Note that  $t_y$  derived from ion implantation experiments is not equal to the total elapsed time on the Moon because a grain will spend variable amounts of time at the surface as the regolith is churned (Gault et al., 1974). For example, the upper 1000  $\mu\text{m}$  of regolith is churned  $\sim 10^3$  times in  $10^7$  years (Gault et al., 1974). If we ignore depth-dependent mixing rates, in this layer a 10- $\mu\text{m}$ -diameter grain would have been exposed at the surface  $(10 \mu\text{m}/1000 \mu\text{m}) \times 10^3 = 10$  times, or a total of  $(10/10^3) \times 10^7 = 10^5$  years out of  $10^7$  elapsed years. An estimate for the total elapsed time for solar wind weathering is  $<10^6$  years in the asteroid belt (Vernazza et al., 2009). If we convert this weathering rate to the value expected at 1 AU (dividing by  $2.5^2$ , Lazarus et al., 1995), we obtain  $1.6 \times 10^5$  years. However, differences in the regolith churn rate and surface chemistry between asteroids and the Moon make such a comparison difficult, and the elapsed time for solar wind weathering on the Moon may be  $>1.6 \times 10^5$  years.

An added complication is that a grain has only a finite chance of being lofted. After each flight, a grain may not land in a position amenable to lofting during the next terminator crossing. Only a crude estimate of the likelihood of lofting is possible using Surveyor data. Using Surveyor optical measurements of dust clouds, Criswell (1972) inferred a lofted mass flux rate equivalent to a soil churn rate of  $\sim 6 \mu\text{m}/\text{year}$ . Therefore, since there are 25 terminator crossing per year, a 6  $\mu\text{m}$  diameter grain has roughly a 1/25 chance of being lofted each crossing. Until more information is available about dust lofting, for simplicity we calculate transport times assuming a lofting probability of 0.1 (two loftings every 295 days).

Two significant unknowns,  $E$  and  $t$ , are explored in Fig. 6 with a range of values. The range of plausible  $E$  values was estimated in Section 3.1 to be 10–100 mV/m. The most conservative estimate of  $t$  is to assume that all lunar dust lofting is not actually stable levitation, but rather ballistic transport up to the height observed by the Surveyor spacecraft (Colwell et al., 2009). Assuming a cloud height of  $\sim 25$  cm (Rennilson and Criswell, 1974) gives a total up and down flight time of  $\sim 1$  s, assuming only the gravity force is a work. However, Pelizzari and Criswell (1978) suggest levitation times of up to hours, and Nitter et al. (1998) and Colwell et al. (2009) report stable levitation modes lasting minutes to hours. Stubbs et al. (2006) suggest high-altitude ballistic flights that may last several minutes. We explore lofting times from 1 s to 10 min.

Fig. 6a and b shows the distance  $d$  for grains of diameter 2 and 10  $\mu\text{m}$  for a range of lofting times. It is clear that dust can travel greater than the required 2–10 km length scale of most swirls, with values of  $E$  and  $t$  that are within the range of plausible values. Because the distance traveled depends linearly on  $E$  and on the square of  $t$ ,  $t$  has a stronger effect on  $d$ . As an intermediate example between the cases plotted, a 6  $\mu\text{m}$  diameter grain at 10 V (charge of  $2.8 \times 10^{-15}$  C) will travel about 1 cm horizontally after a 20 s lofting, in a 10 mV/m field.

### 3.4. Swirl color production

Because the  $<10 \mu\text{m}$  fraction of soil is significant in determining a soil's spectral properties (Noble et al., 2001), horizontal transport

of this fraction has the potential to change a region's band strength and albedo. The most fundamental spectral observations we have to constrain the swirl forming process are: (1) swirl material is higher in albedo, (2) swirl material appears slightly enriched in a component that mimics highlands material, possibly, but not necessarily, with a weak feldspathic enrichment, (3) swirl material apparently has higher band strength than the surrounding material.

The most cohesive hypothesis to explain the above data is that positively (negatively) charged fine dust is being repelled (attracted) into bright areas. Because fine dust is brighter and slightly feldspar rich (Taylor et al., 2001; Pieters and Taylor, 2003), this would explain the first of the two spectral constraints. However, the finest dust (by itself) is also expected to have weak band strength (Taylor et al., 2001), which is in conflict with the third spectral observation. A possible resolution is if the transport process is rapid enough to ensure that newly created dust is deposited and accumulates fast enough to bury material before it weathers, altering the local steady-state equilibrium (McKay et al., 1974). Because we demonstrated that dust can be transported on the timescales of space weathering, this resolution is plausible. A second possible resolution is that the dilution of local materials with finer, more transparent materials increases the optical path length to enhance local absorption bands.

Despite difficulties with the poorly constrained Clementine spectral data, the dust transport model deflects several of the difficulties of the solar wind hypothesis, and is the first to provide a plausible explanation for the apparent highlands component in swirls. It is important to note that a variety of other spectral effects may take place when dust is removed from or emplaced into a region. Many of these effects will be difficult to predict given the complex weathering and mixing processes in the finest fraction of the lunar regolith.

An alternative interpretation that allows for the solar wind stand-off model is given in the Discussion (Section 4.1).

### 3.5. Dark lanes

Electrostatic dust transport also offers a new explanation for the morphology of dark lanes. If there is a small region inside a swirl where there is zero horizontal electric field, dust transport may be close to nonexistent and result in normal soil and weathering. Since the dust transport model above allows for solar wind weathering, the width of the lanes is not limited by the proton gyrodiameter, and can explain the very fine scale of some lanes.

There are two means by which electrostatic anomalies can produce regions of zero horizontal electric field. The first mechanism is that closely adjacent regions of positive electric field may have regions between them where the horizontal component of the field cancels. For example, the horizontal component of the electric field between two positive point charges on a plane is zero, while around this region there are areas of positive electric field. This mechanism may explain the dark lanes between labels B in Fig. 2a, assuming that labels C and Z represent positive charge distributions.

The second mechanism that can produce lanes is if the charge distribution is sufficiently symmetric to yield zero net field in the central regions of the anomaly. For example, the horizontal component of the electric field produced by a cylinder of positive charge, with decreasing radial ( $x$ ) charge density like  $1/x$ , will be exactly zero along its axis, and increase with radius when  $x < R$ , where  $R$  is the cylinder radius. The same holds true for a cylinder cut in half along its central axis. This may explain the narrow dark lanes in Fig. 2a, labels C and D, which are imbedded in bright swirls, assuming an approximately half-cylindrical charge distribution intersects the lunar surface at the rectangles near labels C and D.

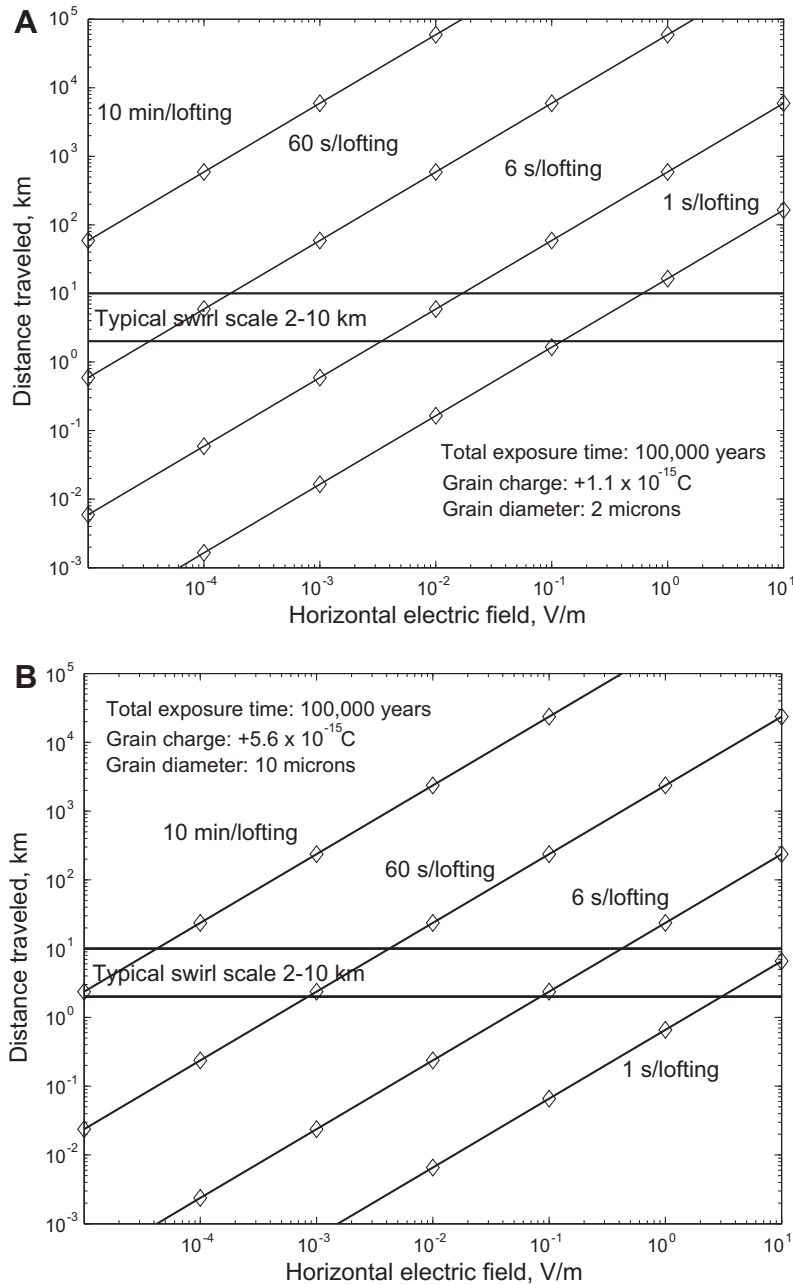


**Fig. 6.** Distance traveled for a grain lofted from the surface and horizontally accelerated by an electric field. The 100,000 year timescale in both figures represents the total time the grain spends exposed on the surface and assumes two loftings every 295 days, equivalent to a lofting probability of 0.1 each lunar day. The typical length scale of most lunar swirls (2–10 km) is indicated. Lofting times from 1 s to 10 min are explored. (A) Grain diameter of 2  $\mu\text{m}$ . (B) Grain diameter of 10  $\mu\text{m}$ .

While the above null-field models for dark lane formation are broadly consistent with observations and the dust transport model, they are admittedly speculative, and cannot be strongly constrained with available data.

## 4. Discussion

### 4.1. Implications

The net result of dust transport is removal or deposition of fine grains from a region. If every  $10^5$  years the minimum 2–10  $\mu\text{m}$  of material are removed or deposited in a swirl region (Section 3.3), the predicted topographic change is only 8–40 cm (assuming minimal packing efficiency) after 4 By, which is the approximate

maximum age of lunar features. This topographic difference may be detectable by careful studies of mare swirls with a sufficiently accurate laser altimeter. However, it is likely that topography of at least several meters would be required to resolve the features in laser altimeter tracks.

Several aspects of the dust transport model and the solar wind stand-off model can be further constrained with high-resolution spectral data that will soon be available. These include, (1) modeling mare swirl spectra as mixtures of fine grained highlands material and mare material (Bell and Hawke, 1987), which requires models that address the nonlinear effects of particle size differences, (2) measuring the spectral properties of dark lanes to constrain their relationship to normal local soil, (3) comparing soil maturity trends within swirls to those of local soils, and (4) measuring young (<100,000 year old) features not affected by the

solar wind, if they can be located, and comparing their spectra with swirl spectra.

One particularly useful test of the dust transport model at lunar swirls would be inferences about particle size differences. Because any fine dust at swirls would likely affect the density, conductivity, and heat capacity of the soil, soil at swirls should exhibit a difference in thermal inertia compared to background values. The thermal inertia can be derived from measurements of infrared temperatures and surface albedos. Ultimately, perhaps the best test of the dust transport model and solar wind stand-off model would be measurements of particle fluxes, electric fields, and dust movement at the surface.

An alternative to the dust transport explanation for swirl spectral properties is that the solar wind stand-off model is at least partially correct, and we do not understand the combined effects of solar wind and micrometeoroid weathering. For example, the solar wind can produce nanophase iron (Hapke, 2001), but micrometeoroid weathering can produce both nanophase iron (Yamada et al., 1999) and change the grain size distribution through comminution. If the solar wind is responsible for a significant portion of the nanophase iron observed in normal soils, and if the solar wind is indeed kept from the surface at magnetic anomalies, then the extreme right portion of Trend 1 may represent fully developed soil produced by micrometeoroid bombardment. This nearly nanophase iron-free soil would be bright, but have the same high abundances of glass welded aggregates and particle size distribution as normal mature soils. Trend 2 is then superimposed on Trend 1 as small craters expose fresh, bright material that is mixed with the local, older and darker soil from Trend 1. Displacements of Trend 1 to the left and right would occur due to increased and decreased solar wind exposure.

The above spectral, topographic, and thermophysical tests may be able to distinguish between the two models, or a combination of the two. Regardless of which model is correct, swirls clearly provide an excellent laboratory to understand the nature of space weathering.

#### 4.2. Applications to other bodies

Other airless solar system objects may produce albedo anomalies like lunar swirls if they have crustal magnetic anomalies. For example, Schultz and Srnka (1980) proposed that albedo anomalies on Mercury may be swirls, and Blewett et al. (2009) have reexamined these anomalies with Messenger data. Vernazza et al. (2006) suggested that Vesta may have a sufficient magnetic field to either stand off the solar wind from the entire body, or to form swirls.

For two reasons, Mercury may not exhibit swirl features under either the solar wind stand-off model or the dust transport model. The first reason is that Mercury has a weak global magnetic field that produces a magnetosphere that is substantially different from the daytime plasma environment on the Moon (Anderson et al., 2009). If the solar wind cannot reach the surface in significant quantities, the generation of electric fields at magnetic anomalies will not occur in the dust transport model, and the local difference in weathering under the solar wind stand-off model will be absent. The actual rate of solar wind weathering on Mercury is, however, still unknown (Noble and Pieters, 2003; Slavin et al., 2007; Denevi and Robinson, 2009). A second, probably less significant reason is that the subsurface temperature on Mercury is higher than on the Moon. For example, the mean diurnal near-surface temperature at Mercury's equator (100–200 °C) is about 120–220 °C higher than on the Moon (–20 °C) (Vasavada et al., 1999). Therefore, after billions of years, magnetic minerals may thermally unblock greater amounts of magnetization on Mercury than on the Moon, and any local crustal magnetic anomalies may be relatively weaker.

Swirls on asteroids do not suffer from the above two difficulties for Mercury. However, the mechanisms by which crustal magnetic anomalies are generated, such as the antipodal convergence of impact ejecta in a magnetic field (Hood and Artemieva, 2008), and cooling of magnetic material in a dynamo field (Weiss et al., 2008), are less well-explored on asteroids than for the Moon. It remains to be seen if swirls will be located on asteroids.

## 5. Conclusions

We have shown (1) swirls exhibit linearly displaced spectral weathering trends, unlike a normal immature surface, which may suggest an increased feldspathic component, (2) dark lane widths and estimated proton gyrodiameters suggest volume magnetizations at least as strong as the most magnetic Apollo samples, if the solar wind stand-off model is correct, (3) fine, electrostatically lofted dust can be transported horizontally by weak electric anomalies created by the solar wind interaction with magnetic anomalies, over distances comparable to swirl length scales, within the solar wind weathering timescale of 100,000 years, assuming parameters derived from Apollo surface measurements and theory, (4) horizontal transport of fine dust can alter the surface spectral properties because it is bright and slightly enriched in feldspathic material. An alternative explanation for the spectral observations is that the solar wind stand-off model is correct, and our understanding of space weathering is incomplete. More swirls on the Moon, and possibly Mercury and asteroids, may be discovered using our results.

The dust transport model for swirl formation accommodates magnetic fields, permits micrometeoroid and solar wind weathering, and can be tested with high-resolution topography data, spectral data, and thermal inertia studies. Ultimately, the best test may be to obtain measurements of magnetic fields, electric fields, dust movement, and particle fluxes at the surface.

## References

- Alfvén, H., Fälthammer, C.G., 1963. *Cosmical Electrodynamics*. Clarendon, Oxford, UK.
- Anderson, B.J. et al., 2009. The magnetic field of Mercury. *Space Sci. Rev.* 152, 307–339.
- Barnes, A., Cassen, P., Mihalov, J.D., Eviatar, A., 1972. Permanent lunar surface magnetism and its deflection of the solar wind. *Science* 172, 716–718.
- Bell, J.F., Hawke, B.R., 1987. Recent comet impacts on the Moon: The evidence from remote-sensing studies. *Publ. Astron. Soc. Pac.* 99, 862–867.
- Berg, O.E., 1978. A lunar terminator configuration. *Earth Planet. Sci. Lett.* 39, 377–381.
- Berg, O.E., Wolf, H., Rhee, J., 1976. Lunar soil movement registered by the Apollo 17 cosmic dust experiment. In: *Interplanetary Dust and Zodiacal Light*, 31st. Springer-Verlag, pp. 233–237.
- Bertaux, J.-L. et al., 2005. Discovery of an aurora on Mars. *Nature* 435, 790–794.
- Bhardwaj, A., Gladston, G.R., 2000. Auroral emissions of the giant planets. *Rev. Geophys.* 38, 295–353.
- Blewett, D.T., Hawke, B.R., Lucey, P.G., 2005a. Lunar optical maturity investigations: A possible recent impact crater and a magnetic anomaly. *J. Geophys. Res.* 110, E04015.
- Blewett, D.T., Hawke, B.R., Richmond, N.C., Hughes, A.L.H., 2005b. A magnetic anomaly associated with an albedo feature near Airy crater in the lunar nearside highlands. *Geophys. Res. Lett.* 34, L24206.
- Blewett, D.T., Hughes, C.G., Hawke, B.R., Richmond, N.C., 2007. Varieties of lunar swirls. *Lunar Planet. Sci. XXXVIII*, Abstract 1232.
- Blewett, D.T., Denevi, B.W., Robinson, M.S., Purucker, M.E., 2009. Do lunar-like swirls occur on Mercury? *Lunar Planet. Sci. XXXX*, Abstract 1352.
- Borisov, N., Mall, U., 2006. Charging and motion of dust grains near the terminator of the Moon. *Planet. Space Sci.* 54, 572–580.
- Brunetto, R., Strazzulla, G., 2005. Elastic collisions in ion irradiation experiments: A mechanism for space weathering of silicates. *Icarus* 179, 265–273.
- Brunetto, R. et al., 2006. Space weathering of silicates simulated by nanosecond pulse UV excimer laser. *Icarus* 180, 546–554.
- Burke, W.J., Reiff, P.H., 1975. The effect of local magnetic fields on the lunar photoelectron layer while the Moon is in the plasma sheet. *Proc. Lunar Sci. Conf.* 6, 2985–2997.

- Campbell, B.A.C.L.M., Campbell, D.B., Hawke, B.R., Ghent, R.R., Margot, J.L., 2006. 20-m resolution radar studies of the Aristarchus Plateau and Reiner Gamma formation. *Lunar Planet. Sci. XXXVII*, Abstract 1717.
- Charles, C., 2007. A review of recent laboratory double layer experiments. *Plasma Sources Sci. Technol.* 16, R1–R25.
- Chevrel, S.P. et al., 2006. Surface physical properties of the lunar regolith at Reiner Gamma: Characterization and distribution using Hapke model inversion. *Lunar Planet. Sci. XXXVII*, Abstract 1173.
- Clay, D.R., Goldstein, B.E., Neugebauer, M., Snyder, C.W., 1975. Lunar surface solar wind observations at Apollo 12 and Apollo 15 sites. *J. Geophys. Res.* 80, 1751–1760.
- Collinson, D.W., 1983. *Methods in Rock Magnetism and Palaeomagnetism: Techniques and Instrumentations*. Chapman and Hall, New York, 503 pp.
- Colwell, J.E. et al., 2007. Lunar surface: Dust dynamics and regolith mechanics. *Rev. Geophys.* 45, RG2006.
- Colwell, J.E. et al., 2009. Lunar dust levitation. *J. Aeros. Eng.* 22, 2–9.
- Criswell, D.R., 1972. Lunar dust motion. *Proc. Lunar Sci. Conf.* 3, 2671–2680.
- Criswell, D.R., De, B.R., 1977. Intense localized photoelectric charging in the lunar sunset terminator region: 2. Supercharging at the progression of sunset. *J. Geophys. Res.* 82, 1005–1007.
- Denevi, B.W., Robinson, M.S., 2009. Albedo of immature mercurian crustal materials: Evidence for the presence of ferrous iron. *Lunar Planet. Sci. XXXIX*, Abstract 1750.
- Dyal, P.C.W., Sonett, C.P., 1970. Apollo 12 magnetometer: Measurements of a steady magnetic field on the surface of the Moon. *Science* 196, 762–764.
- El-Baz, F., 1972. The Alhazen to Abul Wafa swirl belt: An extensive field of light-colored, sinuous markings. In: *Apollo 16 Preliminary Science Report*, NASA SP-315, 29–97.
- Ergun, R.E., Andersson, L., Main, D., Su, Y.-J., Newman, D.L., Goldman, M.V., Carlson, C.W., Hull, A.J., McFadden, J.P., Mozer, F.S., 2004. Auroral particle acceleration by strong double layers: Upward current region. *J. Geophys. Res.* 109, A12220.
- Farrell, W.M. et al., 2007. Complex electric fields near the lunar terminator: The near-surface wake and accelerated dust. *Geophys. Res. Lett.* 34, L14201.
- Ferraro, V.C.A., 1952. On the theory of the first phase of a geomagnetic storm: A new illustrative calculation based on an idealized (plane not cylindrical) model field distribution. *J. Geophys. Res.* 57, 15–49.
- Fuller, M., Cisowski, S.M., 1987. Lunar paleomagnetism. *Geomagnetism* 2, 307–455.
- Gault, D.E., Horz, F., Brownlee, D.E., Hartung, J.B., 1974. Mixing of the lunar regolith. *Proc. Lunar Sci. Conf.* 5, 2365–2386.
- Goertz, C.K., 1989. Dusty plasmas in the Solar System. *Rev. Geophys.* 27, 271–292.
- Goldstein, B., 1974. Observations of electrons at the lunar surface. *J. Geophys. Res.* 79, 23–35.
- Halekas, J.S. et al., 2001. Mapping of crustal magnetic anomalies on the lunar near side by the Lunar Prospector electron reflectometer. *J. Geophys. Res.* 106, 27841–27852.
- Halekas, J.S., Lin, R.P., Mitchell, D.L., 2005. Large negative lunar surface potentials in sunlight and shadow. *Geophys. Res. Lett.* 32, L09102.
- Halekas, J.S. et al., 2008. Lunar Prospector observations of the electrostatic potential of the lunar surface and its response to incident currents. *J. Geophys. Res.* 113, A09102.
- Hapke, B., 2001. Space weathering from Mercury to the Asteroid Belt. *J. Geophys. Res.* 106, 10039–10073.
- Hood, L.L., 1980. Bulk magnetization properties of the Fra Mauro and Reiner Gamma formations. *Proc. Lunar Sci. Conf.* 11, 1879–1896.
- Hood, L.L., Artemieva, N.A., 2008. Antipodal effects of lunar basin-forming impacts: Initial 3-D simulations and comparisons with observations. *Icarus* 193, 485–502.
- Hood, L.L., Schubert, G., 1980. Lunar magnetic anomalies and surface optical properties. *Science* 208, 49–51.
- Hood, L.L., Williams, C.R., 1989. The lunar swirls: Distribution and possible origins. *Proc. Lunar Sci. Conf.* 19, 99–113.
- Hood, L.L., Coleman, P.J., Wilhelms, D.E., 1979. Lunar nearside magnetic anomalies. *Proc. Lunar Sci. Conf.* 10, 2235–2257.
- Hood, L.L. et al., 2001. Initial mapping and interpretation of lunar crustal magnetic anomalies using Lunar Prospector magnetometer data. *J. Geophys. Res.* 106, 27825–27839.
- Hughes, A.L.H., Colwell, J.E., DeWolfe, A.W., 2008. Electrostatic dust transport on Eros: 3-D simulations of pond formation. *Icarus* 195, 630–648.
- Hull, A.J., Bonnell, J.W., Mozer, F.S., Scudder, J.D., Chaston, C.C., 2003. Large parallel electric fields in the upward current region of the aurora: Evidence for ambipolar effects. *J. Geophys. Res.* 108, 1265.
- Kaydash, V. et al., 2009. Photometric anomalies of the lunar surface studied with SMART-1 AMIE data. *Icarus* 202, 393–413.
- Kreslavsky, M.A., Shkuratov, Y.G., 2003. Photometric anomalies of the lunar surface: Results from Clementine data. *J. Geophys. Res.* 108, 5015.
- Kurata, M. et al., 2005. Mini-magnetosphere over the Reiner Gamma magnetic anomaly region on the Moon. *Geophys. Res. Lett.* 32, L24205.
- Lazarus, A.J. et al., 1995. Recent observations of the solar wind in the outer heliosphere. *Adv. Space Res.* 16, 77–84.
- Lin, R.P., 1979. Constraints on the origins of lunar magnetism from electron reflectometer measurements of surface magnetic fields. *Phys. Earth Planet. Inter.* 20, 271–280.
- Lin, R.P. et al., 1998. Lunar surface magnetic fields and their interaction with the solar wind: Results from Lunar Prospector. *Science* 281, 1480–1484.
- Lucey, P.G., Blewett, D.T., Taylor, G.J., Hawke, B.R., 2000. Imaging of lunar surface maturity. *J. Geophys. Res.* 105, 20377–20386.
- Lucey, P. et al., 2006. Understanding the lunar surface and space–Moon interactions. *Rev. Mineral. Geochem.* 60, 83–219.
- Lundin, R. et al., 2006. Plasma acceleration above martian magnetic anomalies. *Science* 311, 890–893.
- Manka, R.H., 1973. Plasma and potential at the lunar surface. In: *Photon and Particle Interactions with Surfaces in Space*, Proceedings of the 6th ESLAB Symposium, Noordwijk, pp. 347–361.
- McCoy, J.E., 1976. Photometric studies of light scattering above the lunar terminator from Apollo solar corona photography. *Proc. Lunar Sci. Conf.* 7, 1087–1112.
- McKay, D.S., Fruland, R.M., Heiken, G.H., 1974. Grain size and evolution of the lunar soil. *Proc. Lunar Sci. Conf.* 5, 887–906.
- Murphy, T.W. et al., 2010. Long-term degradation of optical devices on the Moon. *Icarus* 208, 31–35.
- Neugebauer, M., Snyder, C.W., Clay, D.R., Goldstein, B.E., 1972. Solar wind observations on the lunar surface with the Apollo-12 ALSEP. *Planet. Space Sci.* 20, 1577–1591.
- Nicholas, J.B., Purucker, M.E., Sabaka, T.J., 2007. Age spot or youthful marking: Origin of Reiner Gamma. *Geophys. Res. Lett.* 34, L02205.
- Nitter, T., Havnes, O., Melandso, F., 1998. Levitation and dynamics of charged dust in the photoelectron sheath above surfaces in space. *J. Geophys. Res.* 103, 6605–6620.
- Noble, S.K., Pieters, C.M., 2003. Space weathering on Mercury: Implications for remote sensing. *Solar Syst. Res.* 37, 34–39.
- Noble, S.K. et al., 2001. The optical properties of the finest fraction of lunar soil: Implications for space weathering. *Meteorit. Planet. Sci.* 36, 31–42.
- Page, T.T., Carruthers, G.R., 1978. Far ultraviolet atlas of the large Magellanic Cloud. *Naval Research Laboratory Report* 8206, 1–131.
- Pelizzari, M.A., Criswell, D.R., 1978. Lunar dust transport by photoelectric charging at sunset. *Proc. Lunar Sci. Conf.* 9, 3225–3237.
- Pieters, C.M., Taylor, L.A., 2003. Systematic global mixing and melting in lunar soil evolution. *Geophys. Res. Lett.* 98, 2048.
- Pieters, C.M., Fischer, E.M., Rode, O.A.B., 1993. Optical effects of space weathering: The role of the finest fraction. *J. Geophys. Res.* 98, 20817–20824.
- Pinet, C.P. et al., 2000. Local and regional lunar regolith characteristics at Reiner Gamma Formation: Optical and spectroscopic properties from Clementine and Earth-based data. *J. Geophys. Res.* 105, 9457–9475.
- Pinet, P.C., Cord, A., Chevrel, S., Daydou, Y., 2004. Optical response and surface physical properties of the lunar regolith at Reiner Gamma formation from Clementine orbital photometry: Derivation of the Hapke parameters at local scale. *Lunar Planet. Sci. XXXV*, Abstract 1660.
- Raadu, M.A., 1989. The physics of double layers and their role in astrophysics. *Phys. Rep.* 178, 25–97.
- Reasoner, D.L., Burke, W.J., 1972. Characteristics of the lunar photoelectron layer in the geomagnetic tail. *J. Geophys. Res.* 77, 6671–6687.
- Reiff, P.H., 1975. Modification of particle fluxes at the lunar surface by electric and magnetic fields. *Physics, Astronomy and Astrophysics*. Houston, Rice University, Ph.D.
- Reiff, P.H., Burke, W.J., 1976. Interactions of the plasma sheet with the lunar surface at the Apollo 14 site. *J. Geophys. Res.* 81, 4761–4764.
- Rennilson, J.J., Criswell, D.R., 1974. Survey observations of lunar horizon-glow. *Moon* 10, 121–142.
- Richmond, N.C., Hood, L.L., 2008. A preliminary global map of the vector lunar crustal magnetic field based on Lunar Prospector magnetometer data. *J. Geophys. Res.* 113, E02010.
- Richmond, N.C. et al., 2003. Correlation of a strong lunar magnetic anomaly with a high-albedo region of the Descartes mountains. *Geophys. Res. Lett.* 30, 1395.
- Richmond, N.C. et al., 2005. Correlations between magnetic anomalies and surface geology. *J. Geophys. Res.* 110, E05011.
- Riner, M.A., Robinson, M.S., Eckart, J.M., Desch, S.J., 2008. Global survey of color variations on 433 Eros: Implications for regolith processes and asteroid environments. *Icarus* 198, 67–76.
- Robertson, S., Gulbis, A.A.S., Colwell, J., Horányi, M., 2003. Dust grain charging and levitation in a weakly collisional sheath. *Phys. Plasmas* 10, 3874–3880.
- Robinson, M.S., Thomas, P.C., Veveřka, J., Murchie, S., Carcich, B., 2001. The nature of ponded deposits on Eros. *Nature* 413, 396–400.
- Russell, C.T., Lichtenstein, B.R., 1975. On the source of lunar limb compressions. *J. Geophys. Res.* 80, 4700–4711.
- Saito, Y. et al., 2009. Solar wind proton reflection at the lunar surface: Low energy ion measurement by MAP-PACE onboard SELENE (KAGUYA). *Geophys. Res. Lett.* 35, L24205.
- Sasaki, S. et al., 2001. Production of iron nanoparticles by laser irradiation in a simulation of lunar-like space weathering. *Nature* 410, 555–557.
- Sasaki, S., Kurahashi, E., Yamanaka, C., Nakamura, K., 2003. Laboratory simulation of space weathering: Changes of optical properties and TEM/ESR confirmation of nanophase metallic iron. *Adv. Space Res.* 31, 2537–2542.
- Schamel, H., 1986. Electron holes, ion holes and double layers. *Phys. Rep.* 140, 161–191.
- Schultz, P., 1976. *Moon Morphology: Interpretations Based on Lunar Orbiter Photography*. University of Texas Press, 626 pp.
- Schultz, P., Srnka, L., 1980. Cometary collisions on the Moon and Mercury. *Nature* 284, 22–26.
- Severnyi, A.B., Terez, E.I., Zvereva, A.M., 1973. Preliminary results obtained from an astrophotometer installed on Lunokhod-II. *COSPAR-Konstanz*, 25 May–2 June.
- Severnyi, A.B., Terez, E.I., Zvereva, A.M., 1975. The measurements of sky brightness on Lunokhod-2. *Moon* 14, 123–128.

- Shkuratov, Yu., Kaydash, V., Gerasimenko, S., Opanasenko, N., Velikodsky, Yu., Korokhin, V., Videen, G., Pieters, C., 2010. Probable swirls detected as photometric anomalies in Oceanus Procellarum. *Icarus* 208, 20–30.
- Sickafoose, A.A., Colwell, J.E., Horányi, M., Robertson, S., 2002. Experimental levitation of dust grains in a plasma sheath. *J. Geophys. Res.* 107, 1408.
- Singer, S.F., Walker, E.H., 1962a. Electrostatic dust transport on the lunar surface. *Icarus* 1, 112–120.
- Singer, S.F., Walker, E.H., 1962b. Photoelectric screening of bodies in interplanetary space. *Icarus* 1, 7–12.
- Siscoe, G.L., Goldstein, B., 1973. Solar wind interaction with lunar magnetic fields. *J. Geophys. Res.* 78, 6741–6748.
- Slavin, J.A. et al., 2007. MESSENGER: Exploring Mercury's Magnetosphere. *Space Sci. Rev.* 131, 133–160.
- Staid, M.I., Pieters, C.M., 2000. Integrated spectral analysis of mare soils and craters: Applications to eastern nearside basalts. *Icarus* 145, 122–129.
- Starukhina, L.V., Shkuratov, Y.G., 2004. Swirls on the Moon and Mercury: Meteoroid swarm encounters as a formation mechanism. *Icarus* 167, 136–147.
- Strazzulla, G., Dotto, E.B.R., Brunetto, R., Barucci, M.A., Blanco, A., Orofino, V., 2005. Spectral alteration of the Meteorite Epinal (H5) induced by heavy ion irradiation: A simulation of space weathering effects on near-Earth asteroids. *Icarus* 174, 31–35.
- Stubbs, T.J., Vondrak, R.R., Farrell, W.M., 2006. A dynamic fountain model for lunar dust. *Adv. Space Res.* 37, 59–66.
- Takahashi, K., Kaneko, T., Hatakeyama, R., 2008. Double layer created by electron cyclotron resonance heating in an inhomogeneously magnetized plasma with high-speed ion flow. *Phys. Plasmas* 15, 072108.
- Taylor, L.A. et al., 2001. Lunar mare soils: Space weathering and the major effects of surface-correlated nanophase Fe. *J. Geophys. Res.* 106, 27985–27999.
- Thompson, T.W. et al., 1974. A comparison of infrared, radar, and geologic mapping of lunar craters. *Moon* 10, 87–117.
- Vasavada, A.R., Paige, D.A., Wood, S.E., 1999. Near-surface temperatures on Mercury and the Moon and the stability of polar ice deposits. *Icarus* 141, 179–193.
- Vernazza, P. et al., 2006. Asteroid colors: A novel tool for magnetic field detection? The case of Vesta. *Astron. Astrophys.* 451, L43–L46.
- Vernazza, P. et al., 2009. Solar wind as the origin of rapid reddening of asteroid surfaces. *Nature* 458, 993–995.
- Walker, E.H., 1973. The lunar ionosphere and implications for erosion on the Moon. In: *Photon and Particle Interactions with Surfaces in Space, Proceedings of the 6th ESLAB Symposium, Noordwijk*, pp. 521–544.
- Wang, X.H.M., Robertson, S., 2009. Experiments on dust transport in plasma to investigate the origin of the lunar horizon glow. *J. Geophys. Res.* 114, 05103.
- Wang, J., He, X., Cao, Y., 2008. Modeling electrostatic levitation of dust particles on lunar surface. *IEEE Trans. Plasma Sci.* 36, 2459–2466.
- Weiss, B.P. et al., 2008. Magnetism on the angrite parent body and the early differentiation of planetesimals. *Science* 322, 713–716.
- Willis, D.M., 1971. Structure of the magnetopause. *Rev. Geophys. Space Phys.* 9, 953–985.
- Willis, R.F., Anderegg, M., Feuerbacher, B., Fitton, B., 1972. Photoemission and secondary electron emission from lunar surface material. In: *Photon and Particle Interactions with Surfaces in Space, Proceedings of the 6th ESLAB Symposium, Noordwijk*, pp. 389–401.
- Yamada, M. et al., 1999. Simulation of space weathering of planet-forming materials: Nanosecond pulse laser irradiation and proton implantation on olivine and pyroxene samples. *Earth Planets Space* 51, 1255–1265.
- Zhang, Y., Paxton, L.J., Lui, A.T.Y., 2007. Polar rain aurora. *Geophys. Res. Lett.* 34, L20114.
- Zisk, S.H. et al., 1972. Apollo 16 landing site: Summary of Earth-based remote sensing data. *Apollo 16 Preliminary Science Report, NASA Spec. Publ., NASA SP-315, 29, 105–110.*
- Zook, H.A., McCoy, J.E., 1991. Large scale lunar horizon glow and a high altitude lunar dust exosphere. *Geophys. Res. Lett.* 18, 2117–2120.
- Zook, H.A., Potter, A.E., Cooper, B.L., 1995. The lunar dust exosphere and Clementine lunar horizon glow. *Lunar Planet. Sci. XXVI*, 1577–1578 (abstract).